

Millisecond Pulsars Modify the Radio-SFR Correlation in Quiescent Galaxies

Takahiro Sudoh,¹ Tim Linden,^{2,3,4} and John F. Beacom^{3,4,5}

¹*Department of Astronomy, University of Tokyo, Hongo, Tokyo 113-0033, Japan*

²*Stockholm University and the Oskar Klein Centre, Stockholm, Sweden*

³*Center for Cosmology and AstroParticle Physics (CCAPP), Ohio State University, Columbus, OH 43210, USA*

⁴*Department of Physics, Ohio State University, Columbus, OH 43210, USA*

⁵*Department of Astronomy, Ohio State University, Columbus, OH 43210, USA*

sudoh@astron.s.u-tokyo.ac.jp, linden@fysik.su.se, beacom.7@osu.edu
0000-0002-6884-1733, 0000-0001-9888-0971, 0000-0002-0005-2631

The observed correlation between the far-infrared and radio luminosities of star-forming galaxies (SFGs) shows the close connection between star formation and cosmic-ray production. LOFAR recently extended radio observations of the related correlation with star formation rate to lower frequencies (150 MHz), finding a peculiar radio excess in galaxies with high stellar masses and low star-formation rates. We show that recycled/millisecond pulsars (MSPs) can dominate the non-thermal emission in these massive quiescent galaxies and explain the excess. This is supported by recent data suggesting that MSPs can efficiently convert a large fraction of their spin-down power to e^+e^- pairs. We find that MSP-based models provide a significantly improved (formally $> 19\sigma$, though systematic errors dominate) fit to LOFAR data. We discuss implications for the radio-FIR correlation, the observation of radio excesses in nearby galaxies, and local electron and positron observations.

I. INTRODUCTION

The radio–far-infrared (FIR) correlation is a cornerstone in our understanding of star-formation and cosmic-ray physics. Throughout their brief lives, massive stars produce bright radiation that is absorbed by interstellar dust and re-emitted in the FIR. In their violent deaths, these stars produce shocks that accelerate charged particles to GeV and higher energies. These cosmic rays lose energy via hadronic, inverse-Compton, and synchrotron interactions, producing a bright non-thermal radio flux, among other emissions. The close correlation between non-thermal radio and FIR emission has been found over a wide range of galactic masses and star-formation rates [1–18]. A similar correlation has been found between the gamma-ray and FIR fluxes, providing additional support for the cosmic-ray origin of the radio emission [19–21].

The increasingly high precision of radio and infrared measurements has isolated several confounding variables, including environmental effects [22] and AGN contributions [23, 24], and produced resolved analyses of the radio-FIR correlation within galaxies [25–30]. Intriguingly, observations have detected dispersion in the radio-FIR correlation in the least luminous SFGs. Early studies of low-luminosity galaxies found that both the FIR (due to ineffective dust absorption) and radio (due to ineffective cosmic-ray trapping) fluxes fall below predictions based on “calorimetric” models (which require that both ultraviolet photons and cosmic rays lose all their energy in the galaxy). The breakdown of calorimetry implies that a conspiracy of factors must exist to maintain the radio-FIR correlation over such a large dynamic range [31, 32].

Because the FIR flux may not always trace the SFR accurately, many studies have included optical and UV measurements to better probe the physical correlation between star formation and non-thermal emission (e.g., Refs. [33–38]). The radio-SFR correlation is expressed as $L_r \propto \text{SFR}^\alpha$, where L_r is the radio luminosity, and α is the power-law index. Recent observations find α exceeding unity (e.g., [33–35, 37, 38]), which can be attributed to increasing cosmic-ray confinement

in rapidly star-forming systems.

Radio flux measurements of SFGs have been primarily carried out at GHz frequencies, where both thermal and non-thermal components can contribute. LOFAR recently made measurements at 150 MHz [37–40], where the flux is expected to be dominated by non-thermal components, providing a direct probe of cosmic-ray physics. Recently, Gürkan *et al.* [39] (hereafter, G18) combined a model of spectral energy distributions (MAGPHYS [41]) and photometric data from UV to sub-millimeter to calculate the SFR, correcting for modifications to the FIR-SFR relationship in the least luminous galaxies.

Interestingly, G18 observed excess radio emission in galaxies with low star-formation rates, compared to expectations from the radio-SFR correlation. Splitting their galaxy catalog into two components, they found that the trend is most pronounced in galaxies with total stellar masses that exceed $10^{9.5} M_\odot$, indicating that galaxy mass may play an important role in determining the total radio luminosity. While several effects, including contributions from active galactic nuclei (AGN), pulsars, or Type-Ia SN were briefly mentioned, there is, at present, no clear explanation for this observation.

In this work, we propose that radio emission from recycled, millisecond pulsars (MSPs) may significantly contribute to (and even dominate) the radio luminosity of high-mass/low-SFR galaxies. Unlike supernova remnants (SNRs) and normal pulsars, which trace recent star formation, MSPs first evolve through long-lived low-mass X-ray binary (LMXB) phases [42] and then slowly spin down over \sim Gyr timescales [43, 44]. Thus, the MSP luminosity depends on the integrated star-formation rate over the last ~ 1 –10 Gyr.

We produce the first quantitative fit to LOFAR data using models that include MSPs, finding that physically motivated MSP models improve the fit to LOFAR data by $> 19\sigma$. The paper is outlined as follows. In Sec. II, we present theoretical estimates for the radio flux from SNRs, normal pulsars, and MSPs. In Sec. III, we explain our methodology for fitting the LOFAR data. In Sec. IV, we show the results of our analysis, and, in Sec. V, we discuss the implications of our results.

II. THEORETICAL MODELS FOR RADIO EMISSION FROM SNRS AND MSPS

In ordinary galaxies, the dominant source of the diffuse non-thermal radio flux is due to the synchrotron emission of relativistic electrons in weak ($\sim \mu\text{G}$) galactic magnetic fields. Here we consider production within discrete sources. SNRs produce both *primary* electrons in the shock wave and *secondary* electrons through the acceleration and subsequent hadronic interactions of relativistic protons. Pulsars produce relativistic electrons directly in their magnetospheres. In Secs. II A–II D, we estimate the radio emission from each source class, showing that electrons from MSPs can be important in quiescent galaxies. In Sec. II E, we summarize our radio emission model.

A. Supernova Remnants (Primary)

Core-collapse supernovae inject $\sim 10^{51}$ erg of kinetic energy into the ISM, a subdominant fraction of which (roughly $\eta_e^{\text{SN}} \sim 10^{-3}$) is used to accelerate ambient electrons to relativistic energies [45–47]. To calculate the SNR flux in an SFG, we assume an SFR-dependent core-collapse supernova rate of $0.015\psi \text{ yr}^{-1}$ [48], where ψ is the galactic SFR in $M_\odot \text{ yr}^{-1}$. This produces a steady-state electron injection power of:

$$Q_e^{\text{SN, prim.}} = 5 \times 10^{38} \psi \left(\frac{\eta_e^{\text{SN}}}{10^{-3}} \right) \text{ erg s}^{-1}. \quad (1)$$

In Section II E, we discuss the conversion of this electron power into synchrotron emission.

B. Supernova Remnants (Secondary)

SNRs also produce a significant population of non-thermal protons, which carry a much larger fraction ($\eta_p^{\text{SN}} \sim 0.1$) of the supernova kinetic energy. These protons can subsequently interact with the interstellar medium to produce pions, which promptly decay to produce secondary particles, including electrons and positrons (hereafter, electrons). The fraction of proton power transferred to pions is denoted f_{pp} , and depends on the mass, density, and diffusion properties of the specific galaxy. In the Milky Way, measurements of gamma-ray emission indicate f_{pp} is approximately 0.03 [49].

In each collision, approximately 1/6 of the initial proton energy is converted into relativistic electrons, while the rest is converted primarily into secondary protons, neutrinos and gamma rays. Therefore, the total electron power produced via these “secondary” electrons is:

$$Q_e^{\text{SN, sec.}} = 8 \times 10^{37} \psi \left(\frac{f_{pp}}{10^{-2}} \right) \left(\frac{\eta_p^{\text{SN}}}{0.1} \right) \text{ erg s}^{-1}. \quad (2)$$

Thus, the conversion of SNR power to electron power has a total efficiency $\frac{1}{6}\eta_p^{\text{SN}} f_{pp}$. If this exceeds η_e^{SN} , then synchrotron emission from secondary electrons dominates the galactic

synchrotron emission. Because η_p is unlikely to significantly vary between galaxies, the efficiency f_{pp} determines the dominance of primary or secondary electrons. The efficiency f_{pp} is higher for galaxies that can confine cosmic rays longer, and which have higher collision rates between cosmic rays and dense interstellar gas. It is generally expected that f_{pp} eventually approaches unity (the calorimetric limit) in the strong magnetic fields and high densities of the most intensely star-forming galaxies [32, 50].

This transition is consistent with gamma-ray observations of intensely star-forming galaxies, which indicate that the gamma-ray–FIR correlation exceeds unity, with $L_\gamma \propto L_{\text{IR}}^{1.18}$ [20]. This suggests that f_{pp} scales as $\sim \psi^{0.18}$. The value of f_{pp} is also estimated for nearby galaxies: it is $\sim 1\%$ for the Small Magellanic Cloud [48], on the order of 10% for nearby starbursts M82 and NGC253 [51], and may reach unity for ultraluminous infrared galaxies like Arp220 [52]. This indicates that secondary electrons are generally subdominant for ordinary galaxies, but can dominate in starburst sources [32, 53].

In the following, we assume a scaling between f_{pp} and ψ :

$$f_{pp} = \alpha_{pp} \psi^{\beta_{pp}}. \quad (3)$$

This is a simplification, as f_{pp} should in principle be related to multiple parameters such as the gas mass, galactic size, and magnetic field strength. However, we find that the exact modeling of f_{pp} does not significantly affect our conclusions.

C. Normal Pulsars

Neutron stars are born as the remnants of core-collapse supernovae, with a rotational energy on the order of $10^{48} (P_i/150 \text{ ms})^{-2}$ erg, where P_i is the initial rotational period of the pulsar and is commonly assumed to follow a Gaussian distribution centered at 50–300 ms, and with comparable variation [54, 55]. Over their lifetimes, these pulsars spin down, and their rotational energy is released as a relativistic wind of magnetized e^+e^- plasma (the pulsar wind). This interacts with the ambient medium to create a shock where e^+e^- are accelerated to very high energies to produce a pulsar wind nebula (PWN). Recent studies of non-thermal gamma rays around evolved pulsars (“TeV halos”) have shown that pulsars convert a large fraction ($\eta_e^{\text{PSR}} \sim 10 - 30\%$) of their spindown power into e^+e^- pairs [56, 57]. Assuming that the pulsar production rate is equivalent to the supernova rate, we obtain a steady-state electron power:

$$Q_e^{\text{PSR}} = 5 \times 10^{37} \psi \left(\frac{P_i}{150 \text{ ms}} \right)^{-2} \left(\frac{\eta_e^{\text{PSR}}}{0.1} \right) \text{ erg s}^{-1}. \quad (4)$$

By a comparison of Eq. (4) to Eq. (1), the pulsar contribution is subdominant to the primary electron flux from supernovae. However, there are multiple uncertainties (most importantly in η_e^{PSR} and P_i) that may affect this conclusion. In particular, the average value of $(P_i)^{-2}$ is relatively unconstrained by pulsar statistics, which induce significant uncertainties in this estimate (e.g., the Crab pulsar was born with $P_i \sim 20 \text{ ms}$ [58]).

It is important to note that the comparison between SNR and pulsar energetics is also energy-dependent. PWNe typically have a flat radio spectrum ($d \ln F_\nu / d \ln \nu \simeq -0.2$) [59, 60], which indicates that radio-emitting electrons have a hard spectrum ($d \ln N_e / d \ln E_e > -2$), i.e., that most of the energy is contained in higher-energy electrons that typically radiate X-rays. In contrast, SNRs are energetically dominated by low-energy electrons ($d \ln N_e / d \ln E_e < -2$) that typically produce radio emission. Since our study focuses on LO-FAR observations at 150 MHz, SNR contributions are likely more dominant in our study, compared to studies conducted at GHz frequencies. However, because we study only the integrated radio flux at a single frequency, our model cannot, in principle, differentiate these components.

Radio pulsars also directly produce pulsed, beamed radio emission. However, the fraction of the power carried by this emission is negligible, $\sim 10^{-4}$ [61].

D. Recycled/Millisecond Pulsars (MSPs)

The time dependence of MSP cosmic-ray injection is unique compared to every other source of galactic cosmic-rays. While emission from core-collapse SNe and normal pulsars (Eqs. 1, 2, and 4) depends on the current star-formation rate (ψ), MSPs first evolve through long stellar-binary and LMXB phases, and inject cosmic-rays only after a significant time lag. Moreover, MSPs continue to accelerate non-thermal electrons over a long spin-down timescale, with a spin-down power that is relatively constant over $\sim 10(P_i/5 \text{ ms})^2(B_s/10^{8.5} \text{ G})^{-2} \text{ Gyr}$, where B_s is the magnetic field strength. Thus, the cosmic-ray injection from MSPs traces the average star-formation rate ($\bar{\psi}$) over the last ~ 10 Gyrs. Indeed, MSPs are important sources of gamma-ray emission from globular clusters [62, 63] and the Galactic bulge [64, 65], which indicates that they can power old stellar systems.

While $\bar{\psi}$ is not typically known for most galaxies, the total stellar mass (M_*) serves as an excellent tracer of star-formation over long timescales. Indeed, stellar mass is commonly employed as a tracer for the total population of low-mass X-ray binaries (LMXBs), which are the primary progenitors of MSPs [66–69]. We assume that the total power from MSPs (Q^{MSP}) also correlates with the mass.

Because there are significant uncertainties in the transition from the LMXB to MSP phase (and thus their relative rates), we normalize the MSP population using gamma-ray observations of Milky Way MSPs. Recent work by Ref. [70] attempted to address the effect of incompleteness in the observation of dim MSPs, and estimated the total luminosity of galactic MSPs to fall between $(0.5 - 3) \times 10^{38} \text{ erg s}^{-1}$, which is consistent with previous studies [71–73] (see, however, Ref. [74], which finds a smaller value). Here, we normalize the total luminosity as $L_{38}^{\text{MW}} = L_{\text{MSP}}^{\text{MW}}/10^{38} \text{ erg s}^{-1}$. The stellar mass in the Milky Way disk is $5 \times 10^{10} M_\odot$ [75], which suggests the following relation:

$$Q_{\text{total}}^{\text{MSP}} = 2 \times 10^{38} L_{38}^{\text{MW}} \left(\frac{M_*}{10^{10} M_\odot} \right) \left(\frac{\eta_\gamma}{0.1} \right)^{-1} \text{ erg s}^{-1}, \quad (5)$$

where η_γ is the conversion efficiency from spindown power to gamma-ray luminosity, estimated to be $\sim 10\%$ [76].

These estimates do not include a contribution from galactic globular clusters, which might enhance the total gamma-ray luminosity from the galaxy. We note that the Milky Way value may not be typical. Studies of the LMXB population by Ref. [77] found that, while LMXBs are expected to trace stellar mass, the LMXB population of the Milky Way is roughly 2.5 times smaller than a chosen population of nearby Milky Way analogs. In particular, morphological analyses of the M31 galactic bulge indicate that the MSP population of M31 may be up to a factor of 4 larger than expectations based on Milky Way models [70, 78].

The total MSP intensity may also vary between individual galaxies due to evolutionary effects. In particular, the time lag between the birth of binary stars and the production of MSPs is expected to be $\sim \text{Gyr}$, depending on the main-sequence lifetime of the companion star and the length of LMXB phase. Thus, in galaxies that have formed stars relatively recently ($\sim \text{Gyr ago}$), most of binaries may not yet evolved into MSPs. On the other hand, the spindown timescale of MSPs may also vary significantly, depending on the initial parameters P_i and B_s , which may not be common in all environments. Because massive galaxies formed the bulk of their stellar mass more than $\sim 8 - 10 \text{ Gyr ago}$ [79, 80], the spindown power of MSPs might start to be decreasing.

The power and spectrum of electrons produced by MSPs are highly uncertain, both theoretically and observationally. As in the case of normal pulsars, a substantial relativistic electron population is accelerated within the strong electric and magnetic fields of the pulsar magnetosphere. Notably, despite magnetic field strengths that are several orders of magnitude smaller than normal pulsars, the gamma-ray spectrum of MSPs and normal pulsars is almost identical, indicating that they may also accelerate similar electron populations. However, unlike normal pulsars, MSPs rarely produce bright PWNe [81–83], and thus the relativistic electron may not be subsequently accelerated by a termination shock. This also indicates that energy losses of electrons due to the adiabatic expansion of the nebula and synchrotron cooling inside it are much less important for MSPs, allowing a larger fraction of the injected power to be released into the ISM. Thus, it is likely that the ISM electron spectrum produced by MSPs differs substantially from that produced by normal pulsars.

The conversion efficiency η_e^{MSP} is uncertain, and a wide range of values from a few percent to 90% have been tested in the literature. To date, the most stringent constraints on η_e^{MSP} come from observations at TeV scales. A recent study of the globular cluster M15 by the MAGIC collaboration suggests an efficiency less than 30% [84] for a power-law injection, though it should be noted the frequent stellar interaction in the cluster may significantly suppress the particle production by MSPs. [85]. Observational studies of TeV emission around Galactic MSPs suggests that the value of η_e^{MSP} might be $\sim 10\%$ [86]. Importantly, neither of these observations can strongly constrain the efficiency at the GeV scales which are most important for 150 MHz radio observations.

The lack of PWNe around MSPs makes it difficult to con-

strain their non-thermal electron spectra. Previous studies of non-thermal electron production of MSPs have used a diverse set of models [85, 87–94]. The most common spectral model is a power-law with an exponential cutoff, $dN_e/dE_e \propto E_e^{-\alpha} \exp(-E_e/E_{e,\text{cut}})$, with both parameters taking wide ranges of values: $\alpha \simeq 1.5 - 2.5$ and $E_{e,\text{cut}} \simeq 1 - 10^5$ GeV. Another common approach is mono-energetic distributions peaked at values $\sim 10 - 10^5$ GeV. In Ref. [95], the spectrum is fit to simulations of electron escape in polar-cap models [96].

For our analysis, which uses radio emission at only one frequency (150 MHz), changes in the electron spectrum and the electron acceleration efficiency are degenerate. Thus, we absorb the uncertainty in the MSP spectral shape into the parameter η_e^{MSP} , writing the total electron power from MSPs as

$$Q_e^{\text{MSP}} = 2 \times 10^{37} L_{38}^{\text{MW}} \left(\frac{M_*}{10^{10} M_\odot} \right) \left(\frac{\eta_e^{\text{MSP}}}{\eta_\gamma} \right) \text{ erg s}^{-1}. \quad (6)$$

While the contribution of MSPs is sub-dominant in typical galaxies, it becomes important whenever

$$L_{38}^{\text{MW}} \left(\frac{\eta_e^{\text{MSP}}}{\eta_\gamma} \right) \left(\frac{M_*}{10^{10} M_\odot} \right) \left(\frac{\psi}{1 M_\odot \text{ yr}^{-1}} \right)^{-1} \gtrsim 30. \quad (7)$$

For galaxies with low specific SFR (sSFR; SFR/Mass), the contribution of MSPs can even become dominant. Intriguingly, this is the region ($M_* > 10^{9.5} M_\odot$ and $\psi < 10^{-1} M_\odot \text{ yr}^{-1}$) where LOFAR has identified a radio excess.

E. Modeling the Synchrotron Luminosity in SFGs

In previous subsections, we developed quantitative models for the total electron power from each source class, but thus far we have only qualitatively discussed the production of synchrotron radiation from these populations. There are three effects at play. The first is the energy dependence of the electron spectrum, which affects the fraction of the synchrotron power that is emitted at 150 MHz. The critical frequency for synchrotron radiation is given by

$$\nu_c = 80 \left(\frac{E_e}{\text{GeV}} \right)^2 \left(\frac{B}{6 \mu\text{G}} \right) \text{ MHz}, \quad (8)$$

which indicates that GeV-scale electrons are most efficient at producing the 150 MHz radio emission studied here. The fraction of the total electron power that is stored in 150 MHz emitting electrons, χ_{150} , strongly depends on the spectrum injected by sources.

The second effect pertains to competitive electron energy-loss mechanisms, including inverse-Compton scattering, bremsstrahlung, and ionization. The relative contribution of each component can be evaluated from their cooling

timescales (e.g., Ref [97]):

$$\begin{aligned} t_{\text{syn}} &= 2.6 \times 10^8 \text{ yr } \nu_{150}^{-1/2} \left(\frac{B}{6 \mu\text{G}} \right)^{-3/2}, \\ t_{\text{IC}} &= 2.3 \times 10^8 \text{ yr } \nu_{150}^{-1/2} \left(\frac{B}{6 \mu\text{G}} \right)^{1/2} \left(\frac{w_{\text{ISRF}}}{1 \text{ eV cm}^{-3}} \right)^{-1}, \\ t_{\text{brems}} &= 1.1 \times 10^8 \text{ yr } \left(\frac{n_{\text{gas}}}{0.3 \text{ cm}^{-3}} \right)^{-1}, \\ t_{\text{ion}} &= 4.8 \times 10^8 \text{ yr } \nu_{150}^{1/2} \left(\frac{B}{6 \mu\text{G}} \right)^{-1/2} \left(\frac{n_{\text{gas}}}{0.3 \text{ cm}^{-3}} \right)^{-1}, \end{aligned} \quad (9)$$

where ν_{150} is the observation frequency in the unit of 150 MHz and the assigned galactic properties correspond to their average value over the cosmic-ray confinement volume. Also, we assume that inverse-Compton scattering proceeds in the Thomson regime, which is valid for GeV-scale electrons. The total cooling time, t_{cool} , is estimated from the above terms:

$$\frac{1}{t_{\text{cool}}} = \frac{1}{t_{\text{syn}}} + \frac{1}{t_{\text{IC}}} + \frac{1}{t_{\text{brems}}} + \frac{1}{t_{\text{ion}}}. \quad (10)$$

The relative contribution of each target depends on the electron energy, as well as n_{gas} , B , and w_{ISRF} . If we adopt typical Milky Way parameters, e.g., $n_{\text{gas}} \simeq 0.3 \text{ cm}^{-3}$, $B \simeq 6 \mu\text{G}$, and $w_{\text{ISRF}} \simeq 1 \text{ eV cm}^{-3}$, then the electrons that produce 150 MHz radio emission cool primarily via bremsstrahlung. In many galaxies, however, the magnetic field in synchrotron-emitting regions is found to be $B \simeq 10 \mu\text{G}$ under the assumption of cosmic rays and magnetic field equipartition [98] (see, however, an arguments against equipartition models in starburst galaxies [99]), suggesting that synchrotron losses are important. Our focus on quiescent galaxies may motivate adopting target densities more consistent with massive elliptical galaxies that have lower gas densities, $\sim 10^{-2} \text{ cm}^{-3}$ [100], so then bremsstrahlung and ionization losses may become unimportant. However, the magnetic fields of these galaxies are not tightly constrained. We stress that these parameter choices are degenerate with the total cosmic-ray injection power necessary to explain the radio luminosity, which is, itself, only mildly constrained.

The third effect pertains to cosmic-ray escape, which competes with each energy-loss process. In the Milky Way, measurements of radioactive nuclei in the cosmic rays indicate that GeV-scale cosmic rays are confined over a timescale of $t_{\text{esc}} \sim 10^8 \text{ yr}$ [101, 102], which indicates that GeV leptons lose most of their energy, although there are alternative models that suggest much shorter escape times [103, 104]. We note that self-confinement near SNRs [105–110] and PWNe [111] may be important. Specifically, the local diffusion constant near cosmic-ray emission sources is strongly suppressed due to the amplification of turbulent magnetic fields produced by cosmic-ray particles. While the low gas density within SNRs implies that relatively few cosmic-ray protons interact during this period, the magnetic fields within these regions can be high, leading to efficient electron energy loss. In such a scenario, primary cosmic-ray electrons may

efficiently produce synchrotron radiation, even in very small galaxies that do not efficiently confine cosmic-rays within their bulk.

The competition between cooling and escape set the lifetime of cosmic-rays in galaxies to be:

$$\frac{1}{t_{\text{life}}} = \frac{1}{t_{\text{esc}}} + \frac{1}{t_{\text{cool}}}, \quad (11)$$

which is related to the conversion efficiency of the injected electron power to the synchrotron radiation as

$$f_{\text{syn}} = \frac{t_{\text{life}}}{t_{\text{syn}}}, \quad (12)$$

which depends on the cosmic-ray confinement time, magnetic field strength, and radiation/gas densities. Most naively, f_{syn} is expected to be higher for more massive galaxies that confine cosmic rays for longer times. In the following, we assume a scaling between f_{syn} and M_* :

$$f_{\text{syn}} = \alpha_{\text{syn}} \left(\frac{M_*}{10^{10} M_\odot} \right)^{\beta_{\text{syn}}}. \quad (13)$$

In steady state, the radio luminosity of an SFG is the product of the injection rate of non-thermal electrons (Q_e) and f_{syn} . The total 150 MHz luminosity can be expressed as the sum of contributions from different source classes:

$$L_{150} = f_{\text{syn}} \sum_s \chi_{150}^s Q_e^s, \quad (14)$$

where s denotes the source class, Q_e^s is a function of ψ and M_* (Eqs. 1–2, 4, 6), and χ_{150}^s depends on the source electron spectrum and the galactic magnetic field.

Combining Eqs. (1)–(4), (6) and (13)–(14), we represent the components of the radio luminosity with the following functional forms:

$$\begin{aligned} L_{150} &\propto M_*^{\beta_{\text{syn}}} \psi : \text{SNR primary (and normal pulsars)} \\ L_{150} &\propto M_*^{\beta_{\text{syn}}} \psi^{1+\beta_{pp}} : \text{SNR secondary} \\ L_{150} &\propto M_*^{1+\beta_{\text{syn}}} : \text{MSP} \end{aligned} \quad (15)$$

In Sec. IV, we use these to fit the LOFAR data and constrain the free parameters in our model.

Finally, we note that low-frequency radio emission can be affected by free-free absorption by ionized gas. The critical frequency where the free-free optical depth equals unity is:

$$\nu_{\text{ff}} = 7 \text{ MHz} \left(\frac{T_e}{10^4 \text{ K}} \right)^{-1.35/2.1} \left(\frac{\int n_e n_i dl}{100 \text{ cm}^{-6} \text{ pc}} \right)^{1/2.1}, \quad (16)$$

where T_e is the electron temperature, n_e and n_i are the density of electrons and ions, and the integral is taken along the line of sight. For typical galactic densities, the 150 MHz radio emission is not affected, a result that is confirmed observationally [112–116]. However, in dense starburst galaxies, this can significantly reduce the 150 MHz luminosity [117, 118].

III. DATA ANALYSIS

In this section, we develop a method for comparing our models with the LOFAR data. First, in Sec. III A, we briefly describe the dataset used in this work, and then in Sec. III B, we introduce our fitting methodology.

A. Dataset

We utilize the flux densities, SFRs, and stellar masses of 15088 galaxies analyzed by G18. We refer the reader to Ref. [39] for critical information regarding search strategies, catalog choices, and instrumental systematics, but summarize the key features here. G18 obtained flux density measurements for these sources from the HATLAS/NGP field survey, spanning the redshift range $0 < z < 0.6$, and then utilized a multi-step process to isolate SFGs.

First, they identified radio-loud AGN by utilizing the radio source catalog constructed by Ref. [119]. Then, they divided the remaining sources into SFGs, Composite Systems, Seyferts, LINERs, and Ambiguous sources, utilizing a modified BPT-diagram focused on four emission lines: [NII] λ 6584, [SII] λ 6717, H β , OIII λ 5007, and H α . The necessity of a clear detection for each emission line sets a flux threshold that weights the sample toward systems observed at $z \lesssim 0.25$. They fit multi-wavelength photometric data with the MAGPHYS code to derive SFRs (averaged over the last 100 Myr) and the galactic stellar mass. Sources with bad MAGPHYS fits were removed from the analysis. In the end, 3907 SFGs were analyzed by Ref. [39], and we use the same population in the following.

B. Model Comparison

To examine the role that MSPs play in the production of 150 MHz radio emission, we produce several models utilizing the source classes described in Secs. II A through II D. First, we follow G18 and utilize a straightforward model for the radio-SFR correlation:

$$L^{\text{model}} = \alpha \psi^\beta, \quad (17)$$

where β is the index of the correlation, α is a normalization factor, and L^{model} is the expected 150 MHz radio luminosity. For an alternative model, we add a mass-dependent term.

$$L^{\text{model}} = \alpha \psi^\beta M_*^\gamma. \quad (18)$$

In addition to these two empirical models, we construct two physically motivated models based on the source classes discussed in Secs. II A through II D. The first has only terms depending on the prompt SFR, and thus has a functional form:

$$L^{\text{model}} = (a_1 \psi + a_2 \psi^{\beta_{pp}}) M_*^{\beta_{\text{syn}}}, \quad (19)$$

In the second, we add a contribution from MSPs including a mass-dependent component:

$$L^{\text{model}} = [a_1\psi + a_2\psi^{\beta_{pp}} + a_3M_*]M_*^{\beta_{\text{syn}}}. \quad (20)$$

To reduce the number of free parameters, we fix $\beta_{pp} = 0.18$ based on gamma-ray observations, noting that this choice does not affect our conclusions.

Finally, multiple confounding variables may also affect the radio flux in any given galaxy, including additional sources (e.g., sub-dominant AGN activity), or additional sinks (e.g., dense gas). Thus, we introduce an intrinsic dispersion into our model to account for the impact of outliers. Specifically, we assume a probability distribution for the radio luminosity that follows a Gaussian distribution defined as:

$$P_i(L) = \frac{1}{\sqrt{2\pi}\sigma^2} \exp\left(-\frac{|L - L^{\text{model}}|^2}{2\sigma^2}\right), \quad (21)$$

where we define σ to be a combination of the measured uncertainty for each source and a modeling error. Quantitatively, we set $\sigma^2 = (cL^{\text{model}})^2 + L_{\text{err}}^2$, where c is a free parameter that accounts for the intrinsic model dispersion and L_{err} is the 1σ measurement error. We obtain best-fit parameters by minimizing the negative of the log-likelihood, $-\ln \mathcal{L} = -\sum_i \log(P_i)$, where the summation is taken for all sample SFGs. We utilize the IMINUIT code [120] to find the best-fit model and calculate the error matrix for each model parameter. To calculate the best-fit parameters and likelihood values, we use the units [10^{23} W Hz $^{-1}$] for the radio luminosity and [10^{10} M_\odot] for the stellar mass. Notice that while this affects the total quoted likelihood, it does not affect the difference of the log-likelihood values, $\Delta\text{LG}(\mathcal{L})$, among different models.

Many studies of the radio-FIR correlation have analyzed the logarithmic correlation between each luminosity, using logarithmic error bars that relate to the fractional flux of the signal. Here, however, we utilize the true luminosity, because about 20% of the SFGs in our study have best-fit luminosities that are negative (due to instrumental or systematic issues). If a full likelihood profile were available for the measured radio luminosity of each source, either choice should give the same final results. However, as G18 quote only 1σ error bars, the choice of calculating likelihood profiles in linear or logarithmic space can affect the final answer. In Appendix A, we analyze the data by utilizing a fit to the log-luminosity and analyzing only sources with positive luminosity. We find that our main conclusions are unchanged.

Finally, in our best-fit models, we find that 11 sources have a value of $-\ln \mathcal{L}$ larger than 50, representing a 7σ rejection of our models for these sources. In each case, this stems from a source that is significantly brighter than our model prediction. Because alternative methods of producing bright radio emission (such as undetected AGN and galaxy interactions) may be present, we remove such sources from our fit so that they do not bias the relationship. In Appendix B, we include these sources and show that this treatment does not alter our conclusions.

IV. RESULTS

In this section, we present the results of our analysis. In Sec. IV A, we fit the data with empirical power-law models, showing that the inclusion of a mass dependence is significantly preferred but it still fails to fit the low-SFR data. In Sec. IV B, we analyze physically-motivated models and show that the inclusion of MSPs significantly improves the fit to sources in low-SFR and high-mass regime. In Sec. IV C, we discuss the viability of MSP scenario based on the best-fit parameters.

A. Testing the Simple Scaling Models

We first analyze and compare our simple scaling models (Eqs. 17 and 18) with the LOFAR data. The goal of this portion of the analysis is to determine whether total galaxy mass plays an important role in determining the observed radio luminosity.

Figure 1 shows the correlation between the radio luminosity and SFR, splitting our results into four mass bins. The orange points and error bars show the measured radio fluxes and uncertainties for individual SFGs in our sample. The SFR and stellar mass for each SFG are determined from MAGPHYS fits [39, 41]. The gray and blue points correspond to the *predicted best-fit* values for these same SFGs, based on our models (theoretical uncertainties are discussed below).

This analysis shows that a simple scaling between the SFR and the observed radio luminosity (Eq. 17) systematically underpredicts the radio luminosity in galaxies with star-formation rates smaller than $\sim 0.1M_\odot \text{ yr}^{-1}$. Adding a dependence on mass (Eq. 18) adds a large scatter to the radio-SFR correlation and improves the fit.

We note that our likelihood function includes a significant dispersion (see Eq. 21) that is not represented on this plot. This implies that it would be possible for the model with only ψ -scaling to provide an equally good fit to the LOFAR data, even though the $\psi + M_*$ model appears to better match the data in the figure. This could happen in a scenario where the dispersion in the LOFAR data is not related to the galactic mass. We examine this scenario as follows.

In Table I, we calculate the mass dependence in the LOFAR data by comparing the log-likelihood fits of each model. We find that the addition of a mass-dependent term improves the quality of fit to the radio data by $\Delta\text{LG}(\mathcal{L}) = 838$, corresponding to a $\gtrsim 40\sigma$ detection of mass dependence in the radio-SFR correlation. If we restrict our analysis to only quiescent galaxies (132 have sSFR less than 10^{-11} yr^{-1}), we still improve the fit to the data by $\Delta\text{LG}(\mathcal{L}) = 212$. This is notable, because this cut includes only 3% of the galaxy counts (and is often biased towards galaxies with the largest radio uncertainties), but contributes nearly 25% of the total improvement to the log-likelihood. This indicates that the mass dependence of the radio-SFR correlation is most pronounced in galaxies with the lowest current SFRs.

These results are consistent with those of G18, which also found a correlation between luminosity and stellar mass (see

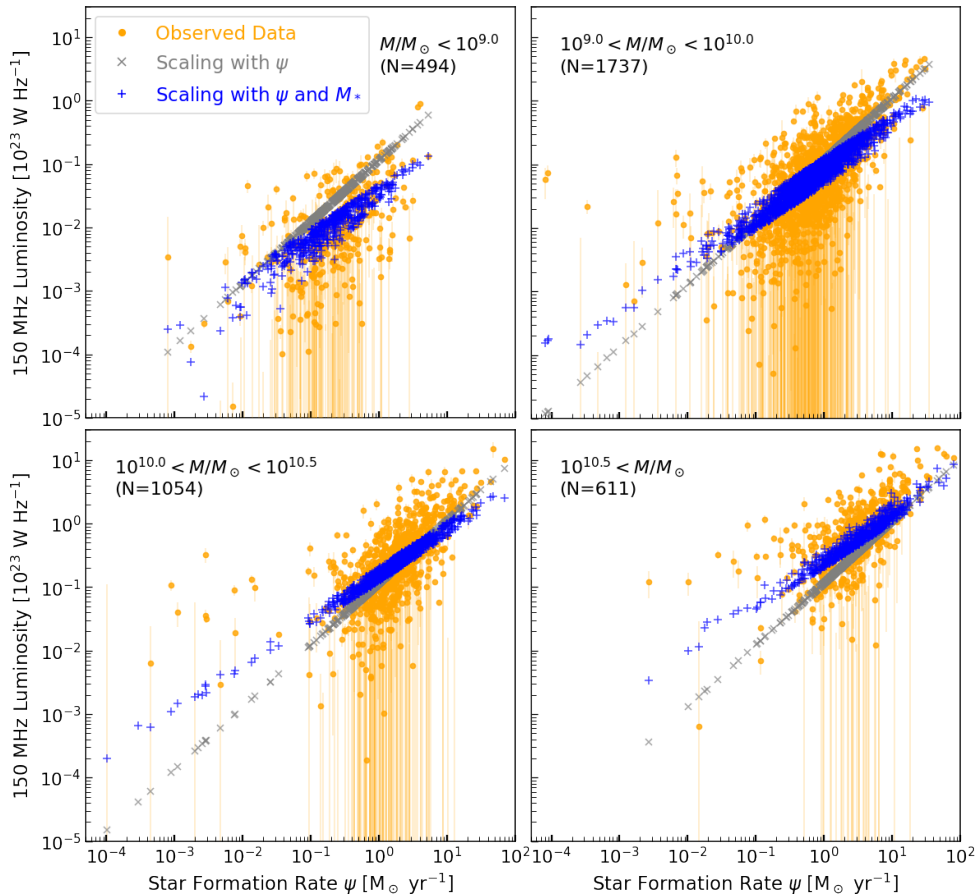


FIG. 1. The 150 MHz luminosity distribution of SFGs as a function of SFR (this and M_* for each source are derived with MAGPHYS). The sample is split into four mass bins as labeled. Orange (circle) points show the observed LOFAR 150 MHz luminosities and 1σ errorbars. Gray (cross) and blue (plus sign) points are the best-fit luminosities predicted by the scaling relations (Eqs. 17 and 18). The model with mass dependence (blue) fits better than prediction by SFR alone (gray), though neither can sufficiently explain low-SFR bright sources.

their Fig. 9). However, our results indicate that even in models that include a mass-dependent term, the predictions of scaling models tend to underestimate the radio luminosity of quiescent galaxies in a systematic fashion.

In Table II, we show the best-fit parameters for both simple scaling models. In our default model, we obtain $\beta = 0.98$, close to the value of unity predicted from the radio-SFR correlation. In our mass-dependent model, β drops to 0.70, an indication that there is degeneracy between the mass and star-formation rate, as expected. The model dispersion, c , is found to be ~ 1.5 for both models, which suggests that the data has an intrinsic variation that spans a factor of ~ 5 at the $\sim 3\sigma$ level. This provides additional evidence that simple scaling models cannot explain bright low-SFR sources. The best-fit parameters derived in our work are similar to those in G18.

B. Testing the Physical Models

Figure 2 compares the two physical models for radio emission, described in Eqs. (19) and (20), with observations. Compared to our simple scaling models, the SNR-only model

TABLE I. Values of $-\ln \mathcal{L}$ for different models. We show the sum of all SFGs (middle) and of low-sSFR SFGs ($< 10^{-11} \text{ yr}^{-1}$, right).

	All Sources ($N = 3896$)	Low sSFR ($N = 132$)
Scaling (ψ ; Eq. 17)	-391.4	258.4
Scaling (ψ and M ; Eq. 18)	-1229.4	46.6
Model (SNR only; Eq. 19)	-894.5	209.5
Model (SNR + MSP; Eq. 20)	-1419.1	-69.3

(light blue, squares) has two additional degrees of freedom, including separate contributions from primary and secondary electrons (with different ψ -dependences), as well as a slight mass dependence relating to the efficiency of synchrotron production. However, this model is still incapable of explaining the bright radio emission from low-SFR sources, implying that the mass-dependent changes in the synchrotron production efficiency are unlikely to explain the observed trend in the data.

Our final model includes a contribution from MSPs, with

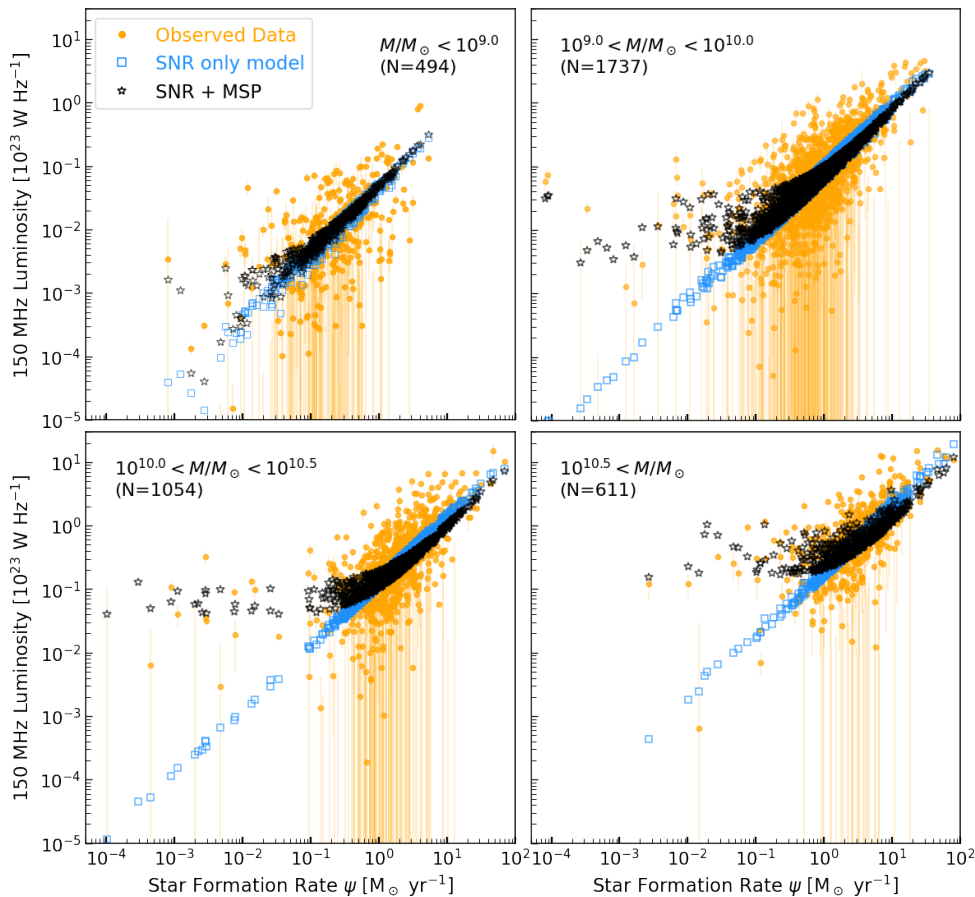


FIG. 2. Same as Fig. 1, but for two physically-motivated models (Eqs. 19 and 20). Light blue (square) points show the model that only includes SNR contribution, which cannot fit the low-SFR data. Black (star) points show the predictions when MSPs are included, which significantly improves the fit to the LOFAR data.

TABLE II. Best-fit parameters for our simple scaling models. In parentheses, we show the best-fit values obtained in G18.

	α	β	γ	c
ψ	0.115 (0.115)	0.976 (1.07)	-	1.51 -
ψ and M_*	0.124 (0.135)	0.702 (0.77)	0.422 (0.43)	1.41 -

a total flux that depends exclusively on the total galactic mass (black, star). Intriguingly, this significantly improves our fit to the radio data, particularly among the population of quiescent galaxies. In Table I, we find that this model improves the log-likelihood fit by 525, producing a 32σ preference for this model compared to the SNR-only model. Restricting our analysis to only galaxies with low sSFR ($< 10^{-11} \text{ yr}^{-1}$), we still find a log-likelihood improvement of 279, corresponding to a 23σ detection even among only the 132 least luminous sources.

We note that our physical SNR-only model provide a worse fit (by a log-likelihood of ~ 306) than our simple scaling

model that depends on ψ and M_* , even though the SNR model has an extra degree of freedom. This is due to the fact that the scaling model prefers a power of ψ that is smaller than one. Such a scenario is incompatible with the assumption of our SNR-only model, because the power of ψ is fixed to either 1.0 or 1.18 for primary (secondary) components. *This indicates that SN driven physics (with an input power that is at least linearly dependent on ψ) is unlikely to drive the radio excess in quiescent galaxies.* Additional factors, such as a competitive energy-loss process (like a cosmic-ray escape component that depends strongly on ψ) would be necessary to explain this data. However, this is not observed in bright SFGs, where the radio-FIR relation is found to be steeper than linear.

In Table III, we list best-fit parameters for our physical models. The normalization for the secondary term, a_2 , is found to be unphysically small for the SNR-only model. This can be understood based on the preference of our scaling model (with ψ and M_*) for a best-fit value $\beta < 1$. Among the two terms that scale as ψ and $\psi^{1.18}$, the best-fit model would only require the first term. This result indicates that our standard SNR model may be unable to provide a good fit to the data. Interestingly, we note that the SNR+MSP model predicts a value of a_2 that is physically reasonable.

TABLE III. Best-fit parameters for our models.

	a_1	a_2	a_3	β_{syn}	c
SNR only	0.110	2.00e-10	-	0.285	1.46
SNR+MSP	0.035	0.031	0.036	0.106	1.39

We should note that there are also sources that are significantly less luminous than our model predictions. However, our models would also predict significant dispersion in the radio luminosity of individual SFGs, which may explain these sources.

In particular, in some systems f_{syn} may be small due to either efficient escape, a strong radiation field, a high gas density, or a weak magnetic field, all of which can lower the synchrotron signal. In addition, free-free absorption may significantly reduce the radio flux in galaxies with high gas densities. Some LOFAR sources even have radio luminosities that are negative, a clear indication of systematic or instrumental effects that are not included in our model. We also note that, contrary to very dim sources, bright sources are difficult to explain solely by a variation in f_{syn} , because it cannot exceed 100%. Finally, we speculate that the star-formation history of each galaxy could stochastically change the total energetics from the population of MSPs, although exact assessment of this effect is difficult.

Our analysis shows that current LOFAR data strongly favor a physical model with mass-dependent cosmic-ray injection (as is clear from Figure. 2). Next, we discuss the validity of the MSP model based on our best-fit parameters.

C. Interpretation of Results

In the previous section, we have shown that the LOFAR data strongly prefers a physical model that includes at least one emission term that depends only on the galaxy mass. In Sec. IID, we noted that a model including MSP-accelerated electrons would predict such a feature. This does not, however, prove that MSPs are the physical source of the excess radio emission. In this section, we show that such a scenario is possible, and, in fact, that current data suggests that MSPs can power bright radio emission with an intensity that is consistent with the excess.

By combining Eqs. (6), (14), (13) and the third term in Eq. (20), we can write the intensity of radio emission from MSPs as:

$$a_3 = \frac{4}{3} \chi_{150}^{\text{MSP}} \alpha_{\text{syn}}^{\text{MSP}} \eta_e^{\text{MSP}} L_{38}^{\text{MW}}, \quad (22)$$

where a_3 is best-fit parameter of the MSP contribution in Eq. (1), χ_{150}^{MSP} is the ratio of the 150 MHz-emitting electron power to the total electron power, and the factor 4/3 arises from the conversion from W Hz^{-1} to erg s^{-1} at 150 MHz. We note that the electron power in the 150 MHz window is calculated over $\Delta \ln E_e = 0.5$, as the luminosity is calculated by integrating the flux density over $\Delta \ln \nu = 1$.

The radio spectral index of galaxies is approximately $F_\nu \propto \nu^{-0.7}$ near GHz frequencies and flattens to $F_\nu \propto \nu^{-0.5}$ near 100 MHz, which is likely caused by cooling and propagation effects [112–116]. This translates to a steady-state differential electron spectrum of $E_e^{-2.4}$ above a few GeV and $E_e^{-2.0}$ below that. Adopting this spectral shape for electrons, we obtain $\chi_{150}^{\text{MSP}} \sim 0.1$, a value that only weakly depends on the spectral break and minimum electron energy.

The efficiency of synchrotron emission, α_{syn} , may also depend on galaxy properties (see Eq. 13). For simplicity, we adopt typical Milky Way parameters to estimate the energy-loss timescales. We also assume that massive galaxies are calorimetric to cosmic-ray leptons, as is the case in the Milky Way [49]. Under these assumptions, we obtain $\alpha_{\text{syn}} \sim 0.2$, which gives us:

$$\eta_e^{\text{MSP}} \simeq 1(L_{38}^{\text{MW}})^{-1}. \quad (23)$$

Thus, we find that the best-fit normalization of the MSP contribution ($a_3 = 0.036$) does not violate the total power of the MSP population. However, since $L_{38}^{\text{MW}} \sim 1$, this relation implies that our model does require the majority ($\eta_e^{\text{MSP}} \sim 1$) of the MSP spindown power to be injected into electrons. This might initially appear worrisome, as some previous estimates have utilized efficiencies of $\eta_e^{\text{MSP}} \sim \eta_\gamma \sim 0.1$. However, there has (to date) been no study validating these assumptions.

Additionally, there are a number of uncertainties in our modeling that may significantly affect this result. Most importantly, the energetics of galactic MSPs are unknown. In this study, we utilized the total gamma-ray luminosity of MSPs normalized to Milky Way observations. However, our MSP models are expected to dominate only in galaxies with low-SFRs and high masses, which may have different star formation histories than the Milky Way. Notably, if we instead chose to normalize our results to M31, which has properties more consistent with quiescent galaxies (a larger stellar mass and a smaller SFR [121, 122]), the necessary MSP efficiency would decrease by up to a factor of ~ 4 . Also, because the gamma-ray emission from MSP magnetosphere may be beamed, only some fraction of Galactic MSPs, f_b , can be observed from the Earth. Although this fraction is often assumed to be $f_b = 1$ for gamma-ray pulsars, the actual value could be smaller by a factor of ~ 2 [123], which would decrease the required η_e^{MSP} by a factor of $1/f_b$. These (among other) uncertainties could significantly lower the necessary efficiencies to $\sim 10\%$ level.

In addition to observational uncertainties that may make the MSP efficiency smaller than what our model predicts, we note that a large e^+e^- efficiency in MSPs is consistent with our current understanding of pulsar physics. Observations indicate that roughly 10% of the MSP spin-down power is converted into gamma-ray emission within the magnetosphere, while a negligible fraction of the total spin-down power is converted to radio, and the remaining power is carried primarily by e^+e^- pairs, the magnetic field, and possibly protons. Although we lack knowledge concerning the energetics of the MSP pulsar wind, in the case of young pulsars, it is established that more than $\sim 90\%$ of the spindown power is converted to pulsar-wind electrons before they create

PWNe [124].

Observationally, the constraints on GeV-scale MSP emission are not strong. Ref. [89] found that e^+e^- efficiencies up to 90% can be reconciled with MSP models of the galactic center excess (see, however, [86]). Intriguingly, studies of GeV emission from the Galactic bulge by Ref. [125] find that the inverse-Compton flux exceeds standard predictions by more than a factor of 20, requiring a bright new source of energetic electrons. At the TeV scale, a stacking analysis of 24 MSPs observed at TeV energies by the HAWC telescope provided 2.6–3.2 σ evidence of TeV MSP emission, a result which would require a high efficiency for TeV e^+e^- pair production from MSPs [86]. We note that observations of globular clusters in very-high-energy gamma rays suggest efficiencies below $\sim 10\%$ [84, 91]. However, this result assumes particularly optimistic models for particle propagation within globular clusters (a Bohmian diffusion model), which has yet to be verified. Extrapolating this result to GeV energies also depends sensitively on spectral assumptions.

In light of these points, we conclude that MSPs can be efficient e^+e^- accelerators. The necessity of an $\mathcal{O}(1)$ e^+e^- efficiency may stretch current modeling. However, multiple uncertainties in MSP population modeling may significantly lower the necessarily efficiencies in models of the radio excess. Furthermore, no observation rules out efficiencies as high as $\sim 90\%$. Next, we discuss the implications and further tests of the model.

V. DISCUSSION AND CONCLUSIONS

In this paper, we propose that MSPs can significantly contribute to the radio flux in quiescent galaxies, dominating the low-end tail of the radio-SFR correlation. We show that models including an MSP contribution significantly improve the fit to LOFAR radio data, explaining the observed excess in low-SFR, high-mass galaxies. Finally, we show that the energetics of our model are consistent with current observations and models of MSP activity. Our results have several implications.

A. Radio-SFR (Radio-FIR) Correlation

Previous studies of the radio-FIR correlation have found a striking continuation of power-law behavior over many orders of magnitude in galactic star-formation rate (e.g., Refs. [6, 9, 10, 31]). This has been attributed to a variety of factors, the sum of which has been labeled a “conspiracy” in the low-SFR behavior of the relationship. LOFAR data, on the other hand, appear to provide evidence for a break in that relationship among high-mass, low-SFR galaxies, and our interpretation offers yet another complicating factor that may shift this relationship from its linear functional form. Our model predicts that future observations of the radio-SFR correlation by LOFAR, as well as next-generation telescopes like SKA, will more clearly identify excess radio emission in high-mass galaxies that do not host AGN.

The tightness of the radio-FIR correlation has raised an expectation that the radio continuum emission can serve as a robust SFR tracer that is not affected by dust extinction. Our analysis suggests that the extrapolation of radio-SFR correlation to low sSFR sources may be insecure, and that future studies of radio emission in low-SFR galaxies should include MSP contributions. Alternatively, more detailed studies of the time-evolution of the MSP population and how it contributes to the galactic radio luminosity may allow radio measurements to inform measurements of star-formation histories in quiescent galaxies.

Finally, the LOFAR data have also been used to perform direct studies of the radio-FIR correlation in 150 MHz band [40]. Based on our results, one would expect excess radio emission for sources that have low FIR luminosity. This is not clearly seen in the data (though the uncertainties in the FIR luminosities for these sources are large). We speculate that this suggests another “conspiracy” in the radio-FIR correlation. For massive galaxies, the radio luminosity is enhanced due to MSPs, and the FIR is also enhanced by the heating of interstellar dust by old stellar populations. Indeed, multiple studies have shown that intermediate and old stellar populations can produce significant IR emission even for galaxies with little star formation [126, 127]. This new conspiracy might be important for future studies.

B. Bright Radio/Gamma-Ray Emission from the Bulge of Disk Galaxies

Although AGN have been removed from the LOFAR sample using BPT-diagram diagnostics, potential radio contributions from relatively-dim supermassive black holes cannot be ruled out. This scenario is particularly troubling, because supermassive black hole masses have been found to correlate with the total galaxy mass [128], providing an alternative explanation for the mass dependence detected in our model (see also G18).

However, nearby, spatially resolved galaxies provide an excellent opportunity to differentiate these scenarios and study the contribution of MSPs to galactic radio emission. If the radio flux is dominantly from AGN, we would expect emission only from the galactic core, and would potentially expect variable emission. On the other hand, MSPs emission would be more extended (although it can be significantly enhanced in the bulge region) and should show no variability.

In addition, observations indicate that LMXBs and MSPs are highly overabundant in dense regions, such as globular clusters, compared to their average formation rate throughout the Milky Way plane [129]. Therefore, cross-correlating diffuse radio emission with globular clusters may provide evidence for an MSP origin of the radio excess.

Intriguingly, there are several nearby galaxies that host both large LMXB populations and also have bright diffuse radio excesses, most notably M31 [78, 130, 131]. Notably, Ref. [131] determined the M31 bulge to be powered by an electron injection of $\sim 10^{39}$ erg s^{-1} , while the SNR population was expected to injection only $\sim 5 \times 10^{37}$ erg s^{-1} .

Utilizing a $M_* = 4 \times 10^{10} M_\odot$ stellar mass for the M31 bulge [70], our model predicts that MSPs inject an electron flux of $\sim 8\eta_e^{\text{MSP}} \times 10^{38} \text{ erg s}^{-1}$, explaining the majority of the electron power.

Variations in the radio-FIR correlation are also seen across the M81 galaxy, with excess radio emission (compared to the Galactic average of Ref. [10]) found outside of active starbursts [132].

C. Implications for Gamma-Ray and Cosmic-Ray Astrophysics

Finally, our results suggest that MSPs may efficiently convert a large fraction of their spin-down power into GeV-scale e^+e^- pairs. Because MSPs do not include compact pulsar wind nebulae, these e^+e^- pairs must escape into the ISM, where they subsequently cool via a combination of synchrotron (producing radio emission) and inverse-Compton scattering/bremsstrahlung (producing gamma-ray emission). The ratio of these components depends sensitively on the galactic environment.

Recent observations have found a bright excess in GeV gamma-ray emission from the Galactic center of the Milky Way galaxy [133, 134]. The most convincing explanations for this excess consist of dark matter annihilation [133, 134] or the production of GeV gamma-ray emission within MSP magnetospheres [135–137]. Our model predicts that any such MSP population will be accompanied by a bright inverse-Compton emission in the Milky Way bulge.

The impact of such a scenario on the interpretation of the Galactic center excess is unclear. At GeV energies, there is some evidence for excess inverse-Compton emission in the Milky Way bulge. In particular, models by the Fermi-LAT collaboration required that the normalization of the inverse-Compton scattering emission from the inner regions of the Milky Way was ~ 20 times brighter than standard Galprop predictions (which, notably, do not include any cosmic-ray injection in the Galactic center region) [125]. Alternative models that do include significant hadronic cosmic-ray injection near the Galactic center include more modest enhancements to the leptonic emission [138].

Our results suggest that GeV-scale e^+e^- from MSPs can significantly contribute to the background gamma-ray emission from the Galactic center, a scenario which may be compatible with MSP models for the Galactic center excess. On the contrary, if the MSP-induced ICS emission continues to TeV energies, the lack of bright TeV emission within the Galactic bulge would place a strong constraint on the contribution of beamed MSP emission to the Galactic center excess at GeV energies [86].

If MSPs do produce bright TeV gamma rays via inverse-Compton scattering, a number of Milky Way MSPs are expected to be local and powerful enough to be seen by current and future TeV telescopes such as HAWC and CTA [86]. Such sources could contribute to the recently discovered population of “TeV Halos” discovered by TeV gamma-ray observations around nearby pulsars like Geminga and Monogem [57, 139],

now also observed at GeV energies [140]. Importantly, unlike normal pulsars, MSPs lack associated SNRs and PWNe, which remain a confounding factor in assessing both the luminosity and morphology of TeV halos. The existence of TeV halo emission surrounding an MSP population would have important implications for our understanding of cosmic-ray propagation near bright TeV emission sources [111].

As an efficient e^+e^- accelerator, MSPs may produce a substantial contribution to the local e^+e^- flux, potentially contributing to the positron excess observed by PAMELA and AMS-02 [141, 142]. While some recent analyses, e.g., Ref. [143] argued that single MSPs explain only a few-percent of the excess, these results assumed electron production efficiencies of only a few percent. On the other hand, Ref. [88] used an efficiency of 50% from spindown power to e^+e^- pairs and found that MSPs can significantly contribute to the observed cosmic-ray electron and positron flux. As our analysis provides additional evidence supporting high e^+e^- efficiencies in MSPs, it supports scenarios where MSPs significantly contribute to the positron excess.

Finally, even in low-SFR galaxies that are supposed to have little astrophysical emission, e^+e^- pairs from MSPs may produce bright radio and gamma-ray emission. This can be additional source of background emission for indirect searches of dark matters. In this context, the contribution from MSPs are evaluated in Ref. [71], but they only consider direct gamma-ray emission from the magnetosphere. Our results suggest that pulsar-wind e^+e^- could significantly contribute to the background emission, potentially making additional factor of confusion for future dark-matter searches. Due to the small size of dwarf galaxies, the luminosity of such a component might depend on the ability for MSPs to self-confine their own cosmic-ray electron population (as in, e.g., TeV halos) [86, 111].

ACKNOWLEDGMENTS

We thank Gulay Gürkan for providing us the data that are used in Ref. [39] and also for providing helpful comments. We also thank Katie Auchettl, Norita Kawanaka, and Todd Thompson for helpful comments. This research made use of ASTROPY [144, 145], MATPLOTLIB [146], NUMPY [147] and IMINUIT [120]. T.S. is supported by a Research Fellowship of Japan Society for the Promotion of Science (JSPS) and by JSPS KAKENHI Grant No. JP 18J20943. T.L. is supported by Swedish Research Council Grant No. 2019-05135. J.F.B. is supported by NSF Grant No. PHY-1714479.

Appendix A: Log-Luminosity

In the main text, we fit our model against the luminosity values and uncertainties for each source using a linear fit to the data. This was due to the fact that some sources have negative best-fit values due to instrumental or systematic issues. Here, we re-analyze the data after taking the logarithm of the luminosity values and uncertainties, producing a probability model given by:

$$P_i(L) = \frac{1}{\sqrt{2\pi\sigma_{\log L}^2}} \exp\left(-\frac{|\log(L) - \log(L^{\text{model}})|^2}{2\sigma_{\log L}^2}\right), \quad (\text{A1})$$

where $\sigma_{\log L}$ is a free parameter. In this analysis, we use only the 3215 sources that have positive best-fit luminosities. In Table IV, we calculate $-\ln \mathcal{L}$ for each model, verifying that the SNR+MSP model fits significantly better than other models. These values cannot be directly compared with those in Table I because the definitions of P_i are different. In particular, while the 1σ error in the uncertainty of each source is identical in both the linear and logarithmic constructions, the likelihood function for any other offset between the modeled and measured source flux will differ.

In Table V, we show the best-fit parameters, showing that they are also not significantly changed, and thus the main physical features of our model are robust to this choice.

TABLE IV. Values of $-\ln \mathcal{L}$ for different models for the case when we use log-luminosity (Eq. A1).

	All Sources ($N = 3215$)	Low sSFR ($N = 108$)
Scaling (ψ ; Eq. 17)	2704	356.7
Scaling (ψ and M ; Eq. 18)	2193	193.3
Model (SNR only; Eq. 19)	2400	384.0
Model (SNR + MSP; Eq. 20)	2050	117.4

TABLE V. Best-fit parameters when we use log-luminosity (Eq. A1).

	α	β	γ	$\sigma_{\log L}$	
Scaling(ψ)	0.108	0.973	-	0.561	
Scaling(ψ and M)	0.127	0.665	0.530	0.479	
	a_1	a_2	a_3	β_{syn}	$\sigma_{\log L}$
Model (SNR only)	0.119	1.06e-9	-	0.351	0.351
Model (SNR+MSP)	0.031	0.046	0.026	0.199	0.458

Appendix B: Bright Sources

In the main text, we removed from our analysis several outliers that had radio luminosities that significantly exceeded model predictions. This is well justified, because other emission sources (e.g, AGN) or additional effects (e.g., galaxy in-

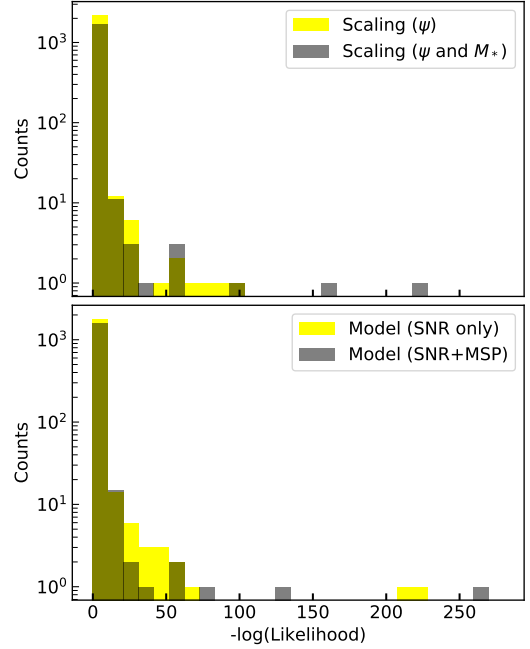


FIG. 3. The distribution of $-\ln \mathcal{L}$ for each SFG. For the scaling model with ψ (top, yellow), there is one source that has $-\ln \mathcal{L} = 989$, which is not shown in this histogram.

teractions) may produce radio excesses that do not correlate with recent or historic star formation.

In Table VI, we show the values of $-\ln \mathcal{L}$ for each model in a scenario where we do not discard these outliers. This confirms that the SNR+MSP models still provide the best fit. However, a comparison of these fits against those in Table I indicates that our fits are highly affected by several very bright sources. In Fig. 3, we show the distribution of the log-likelihood value for individual sources. While most of sources have $-\ln \mathcal{L}$ smaller than 10, some individual sources have $-\ln \mathcal{L}$ more than 50 or even 100. These sources dominate the sum of log-likelihood fit, which could potentially affect our results.

Repeating our analysis, we have verified that our conclusions are unchanged if we set the upper limit for outlier removal to log-likelihood values of 100, 25, and 12.5. In all cases, the SNR+MSP model is favored over any other model by $2\Delta \ln \mathcal{L} > 196$. The best-fit parameters remain largely unchanged.

TABLE VI. Values of $-\ln \mathcal{L}$ for different models for the case when we include all 3097 sources in our analysis.

	All Sources ($N = 3907$)	Low sSFR ($N = 137$)
Scaling (ψ ; Eq. 17)	2625.7	566.3
Scaling (ψ and M ; Eq. 18)	-213.4	17.9
Model (SNR only; Eq. 19)	375.2	312.4
Model (SNR + MSP; Eq. 20)	-580.6	-32.0

- [1] P. C. van der Kruit, *A&A* **29**, 231 (1973).
- [2] P. C. van der Kruit, *A&A* **29**, 263 (1973).
- [3] M. Harwit and F. Pacini, *ApJ* **200**, L127 (1975).
- [4] J. M. Dickey and E. E. Salpeter, *ApJ* **284**, 461 (1984).
- [5] L. J. Rickard and P. M. Harvey, *AJ* **89**, 1520 (1984).
- [6] G. Helou, B. T. Soifer, and M. Rowan-Robinson, *ApJ* **298**, L7 (1985).
- [7] T. de Jong, U. Klein, R. Wielebinski, and E. Wunderlich, *A&A* **147**, L6 (1985).
- [8] E. Hummel, R. D. Davies, R. D. Wolstencroft, J. M. van der Hulst, and A. Pedlar, *A&A* **199**, 91 (1988).
- [9] J. J. Condon, *ARA&A* **30**, 575 (1992).
- [10] M. S. Yun, N. A. Reddy, and J. J. Condon, *ApJ* **554**, 803 (2001), [arXiv:astro-ph/0102154 \[astro-ph\]](#).
- [11] P. N. Appleton *et al.*, *ApJS* **154**, 147 (2004), [arXiv:astro-ph/0406030 \[astro-ph\]](#).
- [12] M. J. Jarvis *et al.*, *MNRAS* **409**, 92 (2010), [arXiv:1009.5390 \[astro-ph.CO\]](#).
- [13] B. Magnelli *et al.*, *A&A* **573**, A45 (2015), [arXiv:1410.7412 \[astro-ph.GA\]](#).
- [14] J. Qiu, Y. Shi, J. Wang, Z.-Y. Zhang, and L. Zhou, *ApJ* **846**, 68 (2017), [arXiv:1708.02687 \[astro-ph.GA\]](#).
- [15] F. S. Tabatabaei *et al.*, *ApJ* **836**, 185 (2017), [arXiv:1611.01705 \[astro-ph.GA\]](#).
- [16] L. Shao, B. S. Koribalski, J. Wang, L. C. Ho, and L. Staveley-Smith, *MNRAS* **479**, 3509 (2018), [arXiv:1806.05447 \[astro-ph.GA\]](#).
- [17] M. E. Filho, F. S. Tabatabaei, J. Sánchez Almeida, C. Muñoz-Tuñón, and B. G. Elmegreen, *MNRAS* **484**, 543 (2019), [arXiv:1811.06577 \[astro-ph.GA\]](#).
- [18] A. Solarz, A. Pollo, M. Bilicki, A. Peł̄spiak, T. T. Takeuchi, and P. Piał̄stek, *PASJ* **71**, 28 (2019), [arXiv:1901.10410 \[astro-ph.GA\]](#).
- [19] M. Ackermann *et al.* (Fermi-LAT), *Astrophys. J.* **755**, 164 (2012), [arXiv:1206.1346 \[astro-ph.HE\]](#).
- [20] T. Linden, *Phys. Rev. D* **96**, 083001 (2017), [arXiv:1612.03175 \[astro-ph.HE\]](#).
- [21] M. Ajello, M. Di Mauro, V. S. Paliya, and S. Garrappa, (2020), [arXiv:2003.05493 \[astro-ph.GA\]](#).
- [22] E. J. Murphy, J. D. P. Kenney, G. Helou, A. Chung, and J. H. Howell, *Astrophys. J.* **694**, 1435 (2009), [arXiv:0812.2922 \[astro-ph\]](#).
- [23] J. J. Condon, W. D. Cotton, and J. J. Broderick, *AJ* **124**, 675 (2002).
- [24] I. Morić, V. Smolčić, A. Kimball, D. A. Riechers, Ž. Ivezić, and N. Scoville, *ApJ* **724**, 779 (2010), [arXiv:1010.0435 \[astro-ph.GA\]](#).
- [25] R. Beck and G. Golla, *A&A* **191**, L9 (1988).
- [26] E. J. Murphy *et al.*, *ApJ* **638**, 157 (2006), [arXiv:astro-ph/0510227 \[astro-ph\]](#).
- [27] R. Paladino, M. Murgia, T. T. Helfer, T. Wong, R. Ekers, L. Blitz, L. Gregorini, and L. Moscadelli, *A&A* **456**, 847 (2006), [arXiv:astro-ph/0606480 \[astro-ph\]](#).
- [28] E. J. Murphy, G. Helou, J. D. P. Kenney, L. Armus, and R. Braun, *Astrophys. J.* **678**, 828 (2008), [arXiv:0801.4768 \[astro-ph\]](#).
- [29] V. Heesen, E. Brinks, A. K. Leroy, G. Heald, R. Braun, F. Bigiel, and R. Beck, *AJ* **147**, 103 (2014), [arXiv:1402.1711 \[astro-ph.GA\]](#).
- [30] V. Heesen *et al.*, *A&A* **622**, A8 (2019), [arXiv:1811.07968 \[astro-ph.GA\]](#).
- [31] E. F. Bell, *Astrophys. J.* **586**, 794 (2003), [arXiv:astro-ph/0212121 \[astro-ph\]](#).
- [32] B. C. Lacki, T. A. Thompson, and E. Quataert, *Astrophys. J.* **717**, 1 (2010), [arXiv:0907.4161 \[astro-ph.CO\]](#).
- [33] J. A. Hodge, R. H. Becker, R. L. White, and W. H. de Vries, *AJ* **136**, 1097 (2008), [arXiv:0806.3986 \[astro-ph\]](#).
- [34] M. J. I. Brown *et al.*, *ApJ* **847**, 136 (2017), [arXiv:1709.00183 \[astro-ph.GA\]](#).
- [35] L. J. M. Davies *et al.*, *MNRAS* **466**, 2312 (2017), [arXiv:1701.06242 \[astro-ph.GA\]](#).
- [36] L. Hindson, G. Kitchener, E. Brinks, V. Heesen, J. Westcott, D. Hunter, H.-X. Zhang, M. Rupen, and U. Rau, *ApJS* **234**, 29 (2018), [arXiv:1801.05348 \[astro-ph.GA\]](#).
- [37] G. Calistro Rivera *et al.*, *MNRAS* **469**, 3468 (2017), [arXiv:1704.06268 \[astro-ph.GA\]](#).
- [38] L. Wang, F. Gao, K. J. Duncan, W. L. Williams, M. Rowan-Robinson, J. Sabater, T. W. Shimwell, M. Bonato, G. Calistro-Rivera, K. T. Chyży, D. Farrah, G. Gürkan, M. J. Hardcastle, I. McCheyne, I. Prandoni, S. C. Read, H. J. A. Röttgering, and D. J. B. Smith, *A&A* **631**, A109 (2019), [arXiv:1909.04489 \[astro-ph.GA\]](#).
- [39] G. Gürkan *et al.*, *MNRAS* **475**, 3010 (2018), [arXiv:1801.02629 \[astro-ph.GA\]](#).
- [40] S. C. Read *et al.*, *MNRAS* **480**, 5625 (2018), [arXiv:1808.10452 \[astro-ph.GA\]](#).
- [41] E. da Cunha, S. Charlot, and D. Elbaz, *MNRAS* **388**, 1595 (2008), [arXiv:0806.1020 \[astro-ph\]](#).
- [42] T. Fragos *et al.*, *ApJ* **764**, 41 (2013), [arXiv:1206.2395 \[astro-ph.HE\]](#).
- [43] R. H. D. Corbet, *A&A* **141**, 91 (1984).
- [44] T. M. Tauris and E. P. J. van den Heuvel, “Formation and evolution of compact stellar X-ray sources,” in *Compact stellar X-ray sources*, Vol. 39 (2006) pp. 623–665.
- [45] V. Tatischeff, *A&A* **499**, 191 (2009), [arXiv:0903.2944 \[astro-ph.HE\]](#).
- [46] J. Park, D. Caprioli, and A. Spitkovsky, *Phys. Rev. Lett.* **114**, 085003 (2015), [arXiv:1412.0672 \[astro-ph.HE\]](#).
- [47] S. K. Sarbadhicary, C. Badenes, L. Chomiuk, D. Caprioli, and D. Huizenga, *MNRAS* **464**, 2326 (2017), [arXiv:1605.04923 \[astro-ph.HE\]](#).
- [48] L. A. Lopez, K. Auchettl, T. Linden, A. D. Bolatto, T. A. Thompson, and E. Ramirez-Ruiz, *ApJ* **867**, 44 (2018), [arXiv:1807.06595 \[astro-ph.HE\]](#).
- [49] A. W. Strong, T. A. Porter, S. W. Digel, G. Jóhannesson, P. Martin, I. V. Moskalenko, E. J. Murphy, and E. Orlando, *ApJ* **722**, L58 (2010), [arXiv:1008.4330 \[astro-ph.HE\]](#).
- [50] T. A. Thompson, E. Quataert, and E. Waxman, *ApJ* **654**, 219 (2007), [arXiv:astro-ph/0606665 \[astro-ph\]](#).
- [51] B. C. Lacki, T. A. Thompson, E. Quataert, A. Loeb, and E. Waxman, *ApJ* **734**, 107 (2011), [arXiv:1003.3257 \[astro-ph.HE\]](#).
- [52] R. D. Griffin, X. Dai, and T. A. Thompson, *ApJ* **823**, L17 (2016), [arXiv:1603.06949 \[astro-ph.HE\]](#).
- [53] B. C. Lacki and R. Beck, *MNRAS* **430**, 3171 (2013), [arXiv:1301.5391 \[astro-ph.CO\]](#).
- [54] C.-A. Faucher-Giguere and V. M. Kaspi, *Astrophys. J.* **643**, 332 (2006), [arXiv:astro-ph/0512585 \[astro-ph\]](#).
- [55] O. C. de Jager, *Astrophys. J.* **678**, L113 (2008), [arXiv:0803.2104 \[astro-ph\]](#).
- [56] D. Hooper, I. Cholis, T. Linden, and K. Fang, *Phys. Rev. D* **96**, 103013 (2017), [arXiv:1702.08436 \[astro-ph.HE\]](#).

- [57] T. Linden, K. Auchettl, J. Bramante, I. Cholis, K. Fang, D. Hooper, T. Karwal, and S. W. Li, *Phys. Rev. D* **96**, 103016 (2017), arXiv:1703.09704 [astro-ph.HE].
- [58] M. Bejger and P. Haensel, *A&A* **405**, 747 (2003), arXiv:astro-ph/0301071 [astro-ph].
- [59] B. M. Gaensler and P. O. Slane, *ARA&A* **44**, 17 (2006), arXiv:astro-ph/0601081 [astro-ph].
- [60] S. P. Reynolds, G. G. Pavlov, O. Kargaltsev, N. Klingler, M. Renaud, and S. Mereghetti, *Space Sci. Rev.* **207**, 175 (2017), arXiv:1705.08897 [astro-ph.HE].
- [61] A. Szary, B. Zhang, G. I. Melikidze, J. Gil, and R.-X. Xu, *ApJ* **784**, 59 (2014), arXiv:1402.0228 [astro-ph.HE].
- [62] A. A. Abdo *et al.*, *Science* **325**, 845 (2009).
- [63] D. Hooper and T. Linden, *J. Cosmology Astropart. Phys.* **2016**, 018 (2016), arXiv:1606.09250 [astro-ph.HE].
- [64] P. L. Gonthier, A. K. Harding, E. C. Ferrara, S. E. Frederick, V. E. Mohr, and Y.-M. Koh, *ApJ* **863**, 199 (2018), arXiv:1806.11215 [astro-ph.HE].
- [65] O. Macias, S. Horiuchi, M. Kaplinghat, C. Gordon, R. M. Crocker, and D. M. Nataf, *J. Cosmology Astropart. Phys.* **2019**, 042 (2019), arXiv:1901.03822 [astro-ph.HE].
- [66] M. Gilfanov, *MNRAS* **349**, 146 (2004), arXiv:astro-ph/0309454 [astro-ph].
- [67] B. D. Lehmer, D. M. Alexander, F. E. Bauer, W. N. Brandt, A. D. Goulding, L. P. Jenkins, A. Ptak, and T. P. Roberts, *ApJ* **724**, 559 (2010), arXiv:1009.3943 [astro-ph.CO].
- [68] B. Boroson, D.-W. Kim, and G. Fabbiano, *ApJ* **729**, 12 (2011), arXiv:1011.2529 [astro-ph.HE].
- [69] T. Fragos *et al.*, *ApJ* **764**, 41 (2013), arXiv:1206.2395 [astro-ph.HE].
- [70] C. Eckner *et al.*, *ApJ* **862**, 79 (2018), arXiv:1711.05127 [astro-ph.HE].
- [71] M. Winter, G. Zaharijas, K. Bechtol, and J. Van den Broeke, *ApJ* **832**, L6 (2016), arXiv:1607.06390 [astro-ph.HE].
- [72] H. Ploeg, C. Gordon, R. Crocker, and O. Macias, *J. Cosmology Astropart. Phys.* **2017**, 015 (2017), arXiv:1705.00806 [astro-ph.HE].
- [73] R. Bartels, E. Storm, C. Weniger, and F. Calore, *Nature Astronomy* **2**, 819 (2018), arXiv:1711.04778 [astro-ph.HE].
- [74] R. T. Bartels, T. D. P. Edwards, and C. Weniger, *MNRAS* **481**, 3966 (2018), arXiv:1805.11097 [astro-ph.HE].
- [75] T. C. Licquia and J. A. Newman, *ApJ* **806**, 96 (2015), arXiv:1407.1078 [astro-ph.GA].
- [76] A. A. Abdo *et al.*, *ApJS* **208**, 17 (2013), arXiv:1305.4385 [astro-ph.HE].
- [77] M. Gilfanov, *Mon. Not. Roy. Astron. Soc.* **349**, 146 (2004), arXiv:astro-ph/0309454.
- [78] M. Ackermann *et al.*, *ApJ* **836**, 208 (2017), arXiv:1702.08602 [astro-ph.HE].
- [79] R. M. McDermid *et al.*, *MNRAS* **448**, 3484 (2015), arXiv:1501.03723 [astro-ph.GA].
- [80] C. Pacifici *et al.*, *ApJ* **832**, 79 (2016), arXiv:1609.03572 [astro-ph.GA].
- [81] B. W. Stappers, B. M. Gaensler, V. M. Kaspi, M. van der Klis, and W. H. G. Lewin, *Science* **299**, 1372 (2003), arXiv:astro-ph/0302588 [astro-ph].
- [82] C. Y. Hui and W. Becker, *A&A* **448**, L13 (2006), arXiv:astro-ph/0601189 [astro-ph].
- [83] J. Lee, C. Y. Hui, J. Takata, and L. C. C. Lin, *A&A* **620**, L14 (2018), arXiv:1811.03284 [astro-ph.HE].
- [84] MAGIC Collaboration, *MNRAS* **484**, 2876 (2019), arXiv:1901.04367 [astro-ph.HE].
- [85] K. S. Cheng, D. O. Chernyshov, V. A. Dogiel, C. Y. Hui, and A. K. H. Kong, *ApJ* **723**, 1219 (2010), arXiv:1009.2278 [astro-ph.HE].
- [86] D. Hooper and T. Linden, *Phys. Rev. D* **98**, 043005 (2018), arXiv:1803.08046 [astro-ph.HE].
- [87] W. Bednarek and J. Sitarek, *MNRAS* **377**, 920 (2007), arXiv:astro-ph/0701522 [astro-ph].
- [88] S. Kisaka and N. Kawanaka, *MNRAS* **421**, 3543 (2012), arXiv:1112.5312 [astro-ph.HE].
- [89] Q. Yuan and K. Ioka, *ApJ* **802**, 124 (2015), arXiv:1411.4363 [astro-ph.HE].
- [90] J. Petrović, P. D. Serpico, and G. Zaharijas, *J. Cosmology Astropart. Phys.* **2015**, 023 (2015), arXiv:1411.2980 [astro-ph.HE].
- [91] W. Bednarek, J. Sitarek, and T. Sobczak, *MNRAS* **458**, 1083 (2016), arXiv:1602.03629 [astro-ph.HE].
- [92] D. Song, O. Macias, and S. Horiuchi, *Phys. Rev. D* **99**, 123020 (2019), arXiv:1901.07025 [astro-ph.HE].
- [93] H. Ndiyavala, C. Venter, T. J. Johnson, A. K. Harding, D. A. Smith, P. Eger, A. Kopp, and D. J. van der Walt, *ApJ* **880**, 53 (2019), arXiv:1905.10229 [astro-ph.HE].
- [94] A. M. Bykov, A. E. Petrov, A. M. Krassilchchikov, K. P. Levenfish, S. M. Osipov, and G. G. Pavlov, *ApJ* **876**, L8 (2019), arXiv:1904.09430 [astro-ph.HE].
- [95] C. Venter, A. Kopp, A. Harding, P. Gonthier, and I. Bsching, *Astrophys. J.* **807**, 130 (2015), arXiv:1506.01211 [astro-ph.HE].
- [96] A. K. Harding and A. G. Muslimov, *ApJ* **743**, 181 (2011), arXiv:1111.1668 [astro-ph.HE].
- [97] A. M. Atoyan, F. A. Aharonian, and H. J. Völk, *Phys. Rev. D* **52**, 3265 (1995).
- [98] R. Beck, L. Chamandy, E. Elson, and E. G. Blackman, *Galaxies* **8**, 4 (2019), arXiv:1912.08962 [astro-ph.GA].
- [99] T. A. Thompson, E. Quataert, E. Waxman, N. Murray, and C. L. Martin, *ApJ* **645**, 186 (2006), arXiv:astro-ph/0601626 [astro-ph].
- [100] W. G. Mathews and F. Brighenti, *ARA&A* **41**, 191 (2003), arXiv:astro-ph/0309553 [astro-ph].
- [101] C. Evoli, G. Morlino, P. Blasi, and R. Aloisio, *Phys. Rev. D* **101**, 023013 (2020), arXiv:1910.04113 [astro-ph.HE].
- [102] G. Morlino and E. Amato, *Phys. Rev. D* **101**, 083017 (2020), arXiv:2003.04700 [astro-ph.HE].
- [103] R. Cowsik and T. Madziwa-Nussinov, *ApJ* **827**, 119 (2016), arXiv:1505.00305 [astro-ph.HE].
- [104] P. Lipari, *Phys. Rev. D* **95**, 063009 (2017), arXiv:1608.02018 [astro-ph.HE].
- [105] Y. Fujita, Y. Ohira, and F. Takahara, *ApJ* **712**, L153 (2010), arXiv:1002.4871 [astro-ph.HE].
- [106] Y. Fujita, F. Takahara, Y. Ohira, and K. Iwasaki, *MNRAS* **415**, 3434 (2011), arXiv:1105.0683 [astro-ph.HE].
- [107] M. A. Malkov, P. H. Diamond, R. Z. Sagdeev, F. A. Aharonian, and I. V. Moskalenko, *ApJ* **768**, 73 (2013), arXiv:1207.4728 [astro-ph.HE].
- [108] L. Nava, S. Gabici, A. Marcowith, G. Morlino, and V. S. Ptuskin, *MNRAS* **461**, 3552 (2016), arXiv:1606.06902 [astro-ph.HE].
- [109] M. D'Angelo, G. Morlino, E. Amato, and P. Blasi, *Mon. Not. Roy. Astron. Soc.* **474**, 1944 (2018), arXiv:1710.10937 [astro-ph.HE].
- [110] K. Fang, X.-J. Bi, and P.-F. Yin, *MNRAS* **488**, 4074 (2019), arXiv:1903.06421 [astro-ph.HE].
- [111] C. Evoli, T. Linden, and G. Morlino, *Phys. Rev. D* **98**, 063017 (2018), arXiv:1807.09263 [astro-ph.HE].
- [112] F. P. Israel and M. J. Mahoney, *ApJ* **352**, 30 (1990).
- [113] E. Hummel, *A&A* **251**, 442 (1991).
- [114] A. Basu, R. Beck, P. Schmidt, and S. Roy, *MNRAS* **449**, 3879

- (2015), arXiv:1503.02420 [astro-ph.GA].
- [115] J. Marvil, F. Owen, and J. Eilek, *AJ* **149**, 32 (2015), arXiv:1408.6296 [astro-ph.GA].
- [116] K. T. Chyży *et al.*, *A&A* **619**, A36 (2018), arXiv:1808.10374 [astro-ph.GA].
- [117] D. F. Torres, *ApJ* **617**, 966 (2004), arXiv:astro-ph/0407240 [astro-ph].
- [118] M. S. Clemens, A. Scaife, O. Vega, and A. Bressan, *MNRAS* **405**, 887 (2010), arXiv:1002.3334 [astro-ph.GA].
- [119] P. N. Best and T. M. Heckman, *MNRAS* **421**, 1569 (2012), arXiv:1201.2397 [astro-ph.CO].
- [120] F. James and M. Roos, *Computer Physics Communications* **10**, 343 (1975).
- [121] J. Yin, J. L. Hou, N. Prantzos, S. Boissier, R. X. Chang, S. Y. Shen, and B. Zhang, *A&A* **505**, 497 (2009), arXiv:0906.4821 [astro-ph.GA].
- [122] J. Sick, S. Courteau, J.-C. Cuilland re, J. Dalcanton, R. de Jong, M. McDonald, D. Simard, and R. B. Tully, in *Galaxy Masses as Constraints of Formation Models*, IAU Symposium, Vol. 311, edited by M. Cappellari and S. Courteau (2015) pp. 82–85, arXiv:1410.0017 [astro-ph.GA].
- [123] T. J. Johnson, C. Venter, A. K. Harding, L. Guillemot, D. A. Smith, M. Kramer, Ö. Çelik, P. R. den Hartog, E. C. Ferrara, X. Hou, J. Lande, and P. S. Ray, *ApJS* **213**, 6 (2014), arXiv:1404.2264 [astro-ph.HE].
- [124] F. V. Coroniti, *ApJ* **349**, 538 (1990).
- [125] M. Ajello *et al.* (Fermi-LAT), *Astrophys. J.* **819**, 44 (2016), arXiv:1511.02938 [astro-ph.HE].
- [126] S. Salim *et al.*, *ApJ* **700**, 161 (2009), arXiv:0905.0162 [astro-ph.CO].
- [127] D. Calzetti *et al.*, *ApJ* **714**, 1256 (2010), arXiv:1003.0961 [astro-ph.CO].
- [128] J. Magorrian *et al.*, *AJ* **115**, 2285 (1998), arXiv:astro-ph/9708072 [astro-ph].
- [129] J. E. Grindlay, *Advances in Space Research* **3**, 19 (1984).
- [130] R. Voss and M. Gilfanov, *A&A* **468**, 49 (2007), arXiv:astro-ph/0610649 [astro-ph].
- [131] A. McDaniel, T. Jeltema, and S. Profumo, *Phys. Rev. D* **100**, 023014 (2019), arXiv:1903.06833 [astro-ph.HE].
- [132] K. D. Gordon *et al.*, *Astrophys. J. Suppl.* **154**, 215 (2004), arXiv:astro-ph/0406064.
- [133] L. Goodenough and D. Hooper, (2009), arXiv:0910.2998 [hep-ph].
- [134] T. Daylan, D. P. Finkbeiner, D. Hooper, T. Linden, S. K. N. Portillo, N. L. Rodd, and T. R. Slatyer, *Phys. Dark Univ.* **12**, 1 (2016), arXiv:1402.6703 [astro-ph.HE].
- [135] K. N. Abazajian, *JCAP* **03**, 010 (2011), arXiv:1011.4275 [astro-ph.HE].
- [136] R. Bartels, S. Krishnamurthy, and C. Weniger, *Phys. Rev. Lett.* **116**, 051102 (2016), arXiv:1506.05104 [astro-ph.HE].
- [137] S. K. Lee, M. Lisanti, B. R. Safdi, T. R. Slatyer, and W. Xue, *Phys. Rev. Lett.* **116**, 051103 (2016), arXiv:1506.05124 [astro-ph.HE].
- [138] E. Carlson, T. Linden, and S. Profumo, *Phys. Rev. D* **94**, 063504 (2016), arXiv:1603.06584 [astro-ph.HE].
- [139] A. U. Abeysekara *et al.*, *Science* **358**, 911 (2017), arXiv:1711.06223 [astro-ph.HE].
- [140] M. Di Mauro, S. Manconi, and F. Donato, *Phys. Rev. D* **100**, 123015 (2019), arXiv:1903.05647 [astro-ph.HE].
- [141] O. Adriani, G. C. Barbarino, G. A. Bazilevskaya, R. Bellotti, M. Boezio, E. A. Bogomolov, L. Bonechi, and PAMELA Collaboration, *Phys. Rev. Lett.* **105**, 121101 (2010), arXiv:1007.0821 [astro-ph.HE].
- [142] M. Aguilar *et al.* (AMS Collaboration), *Phys. Rev. Lett.* **110**, 141102 (2013).
- [143] C. Venter, A. Kopp, A. K. Harding, P. L. Gonthier, and I. Buesching, in *34th International Cosmic Ray Conference (ICRC2015)*, International Cosmic Ray Conference, Vol. 34 (2015) p. 462, arXiv:1508.04676 [astro-ph.HE].
- [144] Astropy Collaboration, *A&A* **558**, A33 (2013), arXiv:1307.6212 [astro-ph.IM].
- [145] Astropy Collaboration, *AJ* **156**, 123 (2018), arXiv:1801.02634 [astro-ph.IM].
- [146] J. D. Hunter, *Computing in Science & Engineering* **9**, 90 (2007).
- [147] S. van der Walt, S. C. Colbert, and G. Varoquaux, *Computing in Science Engineering* **13**, 22 (2011).